

# Observation of Cs Rydberg atom macrodimers

K. R. Overstreet, A. Schwettmann, J. Tallant, D. Booth, and J. P. Shaffer

University of Oklahoma, Homer L. Dodge Department of Physics and Astronomy, 440 W. Brooks St., Norman, OK 73019

(Dated: October 22, 2018)

We report the observation of cold Cs Rydberg atom molecules bound at internuclear separations of  $R \sim 3\text{-}9\ \mu\text{m}$ . The bound states result from avoided crossings between Rydberg atom pair interaction potentials in an applied electric field. The molecular states can be modified by changing the applied electric field. The molecules are observed by mapping the radial separation of the two Rydberg atoms as a function of time delay between excitation and detection using the Coulomb repulsion of the ions after pulsed field ionization. Measurements were performed for  $63D + 65D$ ,  $64D + 66D$ ,  $65D + 67D$ , and  $66D + 68D$  pairs. The experiment is in good agreement with calculations of the pair interactions for these states.

PACS numbers: 34.50.Cx, 32.80.Ee, 82.20.Bc

Frozen Rydberg gases [1, 2] have been the subject of intense research recently. The construction of fast quantum gates and single photon sources using dipole blockade [3, 4, 5, 6, 7, 8, 9, 10], the study of cold Rydberg atom molecules [11, 12, 13, 14], and the investigation of many body physics [1, 2] are central motivations for this work. Cold Rydberg atom molecules are exciting because of the interesting properties that these objects possess. Molecules formed by two cold Rydberg atoms are called macrodimers since the atoms are bound at distances  $> 1\ \mu\text{m}$ . It has been suggested that due to their delicate nature, macrodimers can be used to study vacuum fluctuations, quenching in ultracold collisions [12] and Rydberg atom interactions including their controllability with applied electric fields. Prior experiments have been unable to unambiguously confirm that these unique states of matter exist as bound states [15, 16]. We report the first experimental observation of bound macrodimers which have one of the largest, if not the largest, molecular bond observed to date.

The macrodimers that we observe result from avoided crossings between Rydberg atom pair interaction potentials in an applied electric field,  $\epsilon$  [13]. These

macrodimers are unique because they feature a quasi-continuum of bound states, are found at extremely large internuclear separation,  $R \sim 3\text{-}9\ \mu\text{m}$ , and are formed by the interplay between Van der Waals interactions and the Stark effect resulting from  $\epsilon$ .  $\epsilon$  can be used to stabilize, destroy or modify the potential well that gives rise to the bound states. A spectrum and calculated potentials [17] for the  $65D + 67D$  pair with  $\epsilon = 190\ \text{mV cm}^{-1}$ , are shown in Fig. 1. The potentials have prominent wells at  $R \sim 3\text{-}9\ \mu\text{m}$ . These potential wells support hundreds of bound states [13] with maximum energy spacings of  $\sim 100\ \text{kHz}$ . The lifetimes of the molecules are limited by the radiative and blackbody decay of the atoms [13].

## DETECTING MACRODIMERS

Macrodimers are difficult to detect. Pulsed field ionization (PFI) breaks the molecule apart and complicates time-of-flight (TOF) mass spectrometry. Using selective field ionization to ionize only one of the Rydberg atoms forming the molecule creates an ion close to the remaining Rydberg atom. The electric field of the ion can ionize the atom. Field ionizing both atoms creates two ions that repel each other, causing the complex to dissociate. All these possibilities lead to the detection of singly ionized Cs atoms at the same average TOF. Detection of the molecular ro-vibrational spectrum is difficult because it is a quasi-continuum. For the state shown in Fig. 1, the rotational constant is  $\sim 6\ \text{Hz}$  while the maximum classical angular momentum at the equilibrium separation,  $R_e$ , is  $l_{max} = \mu v R_e / \hbar \approx 310$ .  $\mu$  is the reduced mass and  $v$  is the thermal velocity. Given that the radiative decay time leads to a natural line width of  $\sim 10\ \text{kHz}$  for  $66D$  and taking into account the allowed rotational transitions due to the large impact parameter, each vibrational line will have a width of  $\sim 580\ \text{kHz}$ . This width is much greater than the vibrational energy spacings. Consequently, it is unlikely that the ro-vibrational states of a macrodimer can be resolved unless deeper and narrower

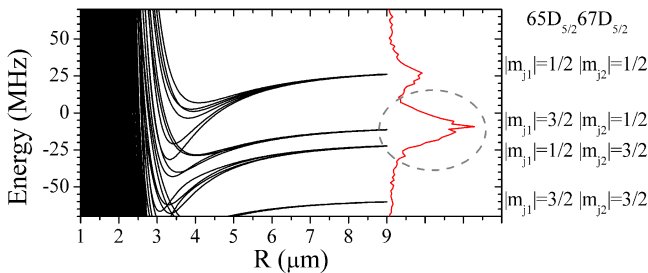


FIG. 1: Integrated atomic ion yield spectra and pair potentials for  $65D + 67D$  with  $\epsilon = 190\ \text{mV cm}^{-1}$ . The excitation laser intensity is  $\sim 500\ \text{W cm}^{-2}$ . All fine structure and  $\Omega$  are plotted.  $\Omega = m_{j1} + m_{j2}$  is the projection of the angular momentum on  $R$ . The dashed line highlights one of the features studied in this paper.

potential wells can be located.

We use the recoil velocity distribution to detect the Cs macrodimers in our experiment [16, 18]. A basic characteristic of a bound state is that the atoms remain in close proximity for a long time compared to the vibrational period. The signature of molecule formation in our experiment is based on this principle. We measure the recoil velocity of the ion fragments after PFI as a function of the delay,  $\tau$ , between excitation and PFI. If two Rydberg atoms are close together and pulsed field ionized, the ions created will Coulomb repel each other. The amount of Coulomb repulsion, which is reflected in the recoil velocity of the ions, is a measure of the  $R$  at which the pair was ionized. Measuring the recoil velocity of the ions as a function of  $\tau$  maps the distribution of radial separations of the two Rydberg atoms as a function of time. For a bound state, the distribution of  $R$  will remain relatively constant as a function of  $\tau$ . For a dissociative process, the distribution of  $R$  will change with  $\tau$ . The recoil velocity can be measured by recording the TOF distribution of the ions that were created by PFI of the molecule at a detector in a TOF experiment [18].

In our experiment, we do not expect to observe oscillations of the Coulomb repulsion due to molecular rovibrational wave-packet motion. The vibrational periods are  $\lesssim 10 \mu\text{s}$ . Experimental limitations such as long term laser stability and excitation pulse average away any oscillations that may be present. Future experiments designed to observe wave-packet motion will be interesting since macrodimers exist at the interface between quantum and classical dynamics.

## EXPERIMENTAL METHODS AND RESULTS

The macrodimers are created in a Cs magneto-optic trap (MOT). The MOT contains  $10^7$  atoms at a density of  $\rho \sim 2 \times 10^{10} \text{ cm}^{-3}$  at a temperature of  $\sim 124 \mu\text{K}$  [18]. The background pressure is  $\sim 5 \times 10^{-10}$  Torr. The MOT is formed between two electric field plates, 26.7 cm above a microchannel plate (MCP) detector. The experimental apparatus is described in more detail in [18].

The Cs macrodimers are excited by a 2-photon scheme

$$6P_{3/2} + 6P_{3/2} + 2h\nu \rightarrow (n-1)D + (n+1)D, \quad (1)$$

where  $n = 64, 65, 66$ , and  $67$ . The MOT trapping light is shut off during the time when the molecules are excited and detected. The MOT repumping light is on during the experiment. The atoms in the  $6P_{3/2}(F=5)$  state are excited from the  $6S_{1/2}(F=4)$  state using a 1 mm spot size beam derived from the trapping laser. This beam is crossed at  $22.5^\circ$  with a beam from a dye laser (Coherent 699) operating at  $\lambda = 508-509 \text{ nm}$  that drives the 2-photon transition in Eq. 1. The dye laser is focused to a  $\sim 25 \pm 10 \mu\text{m}$  spot size that was measured with a

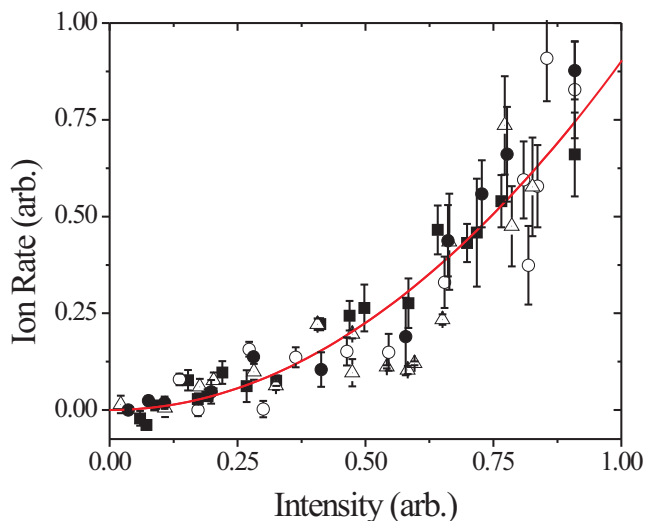


FIG. 2: The rate dependence on excitation laser intensity. Solid triangles ( $\blacktriangle$ ) denote  $63D+65D$  molecular state, open triangles ( $\triangle$ )  $64D+66D$ , open circles ( $\circ$ ) the  $65D+67D$ , and closed squares ( $\blacksquare$ )  $66D+68D$ . Intensities and rates have been normalized to show the quadratic dependence. The solid line is a quadratic fit to the data.

CCD camera. The dye laser polarization is parallel to the TOF axis. The crossed beam geometry helps reduce background counts. The intensity of the dye laser and the trapping light used to excite the atoms to  $6P_{3/2}(F=5)$  is  $500 \text{ W cm}^{-2}$  and  $0.5 \text{ W cm}^{-2}$  respectively.

Bound or free Rydberg atoms are detected in the experiment using PFI. The experiment begins when the trapping light is switched off.  $2.5 \mu\text{s}$  after this light is switched off, the Rydberg excitation beams are turned on for  $5 \mu\text{s}$ . After a variable delay,  $\tau$ , a PFI pulse is applied for  $2 \mu\text{s}$  at an amplitude of  $76 \text{ V cm}^{-1}$  to ionize the Rydberg atoms that were excited and push the ions to the MCP. The rise time of the electric field pulse is  $\sim 80 \text{ ns}$ . A  $153 \text{ mV cm}^{-1} \mu\text{s}^{-1}$ ,  $5 \mu\text{s}$  duration ramp electric field is applied immediately preceding the PFI pulse to clear any stray ions from the excitation region. The atoms move  $< 500 \text{ nm}$  due to thermal motion during this time. The ionized atoms have a TOF distribution centered at  $\sim 27 \mu\text{s}$ . The pulses from the MCP are processed by a constant fraction discriminator and accumulated by a multichannel analyzer. A constant voltage is applied to the upper field plate during excitation to generate  $\epsilon$ . To measure TOF velocity distributions, the sequence was repeated at a rate of  $1 \text{ kHz}$  which resulted in count rates of  $\sim 10 \text{ Hz}$ .

Under the experimental conditions described, many molecular resonances are observed for Rydberg atom pairs at different  $\epsilon$  [13, 16]. In this experiment, we measured molecular resonances for  $63D + 65D$ ,  $64D + 66D$ ,  $65D + 67D$  and  $66D + 68D$  pairs. We focused on these states because our calculations indicated that bound

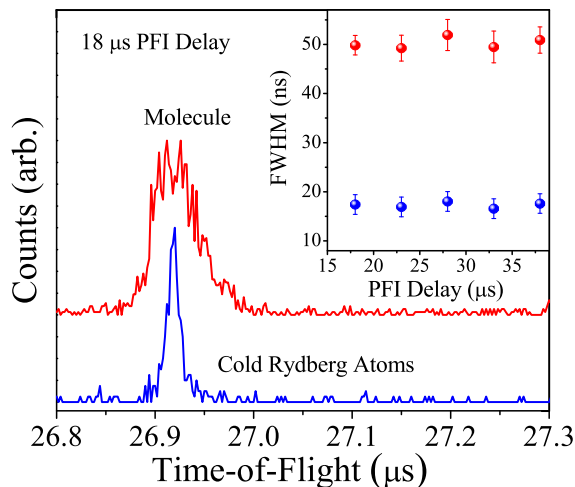


FIG. 3: Comparison of TOF distributions for the 66D atomic case (blue) and the 65D+67D molecular case (red) at  $\tau = 18 \mu\text{s}$ . The horizontal axis is centered on the atomic TOF. These distributions measure the particle velocities or kinetic energies [18]. The inset shows the full width at half maximum of a Gaussian fit to each of the different distributions at different time delays. The atomic data was taken by tuning the laser to the atomic state under conditions of single particle counting.

states existed for certain  $\epsilon$  and these states satisfied the necessary experimental requirements. The experimental considerations are a compromise between an acceptable oscillator strength and the elimination of background counts from Rydberg atoms. The oscillator strength for the molecular excitation is predominantly due to mixing via multipole interactions and electric fields with the nearest atomic state which tends to decrease with increasing energy separation. The asymptotic atomic states are far detuned from the excitation laser frequency so without the mixing one expects little transition strength to the molecular states. However, the noise in the measurement increases with  $n$  as the molecular resonance moves closer to the atomic line wing where some atomic Rydberg excitation occurs.

The excitation rate for each molecular resonance was first measured as a function of excitation laser intensity and found to be quadratic indicating a 2-photon excitation process, Fig. 2. These observations, our prior experiments [16] and the fact that the gas is dilute are evidence that the spectral features are from processes involving two Rydberg atoms. The fact that the spectral features are associated with molecular excitations does not necessarily indicate the presence of macrodimers. Many resonances result from photo-initiated collisions where the atoms are not excited to bound states [16].

Two sample TOF distributions at  $\tau = 18 \mu\text{s}$  are shown in Fig. 3. The inset of Fig. 3 shows the full width at half maximum of a Gaussian fit to each of the distributions for  $\tau = 18 - 38 \mu\text{s}$ . The narrow distribution was obtained by

tuning the excitation laser to the 66D atomic resonance under conditions for single atom counting. The broad distribution was acquired by tuning the excitation laser to the feature circled in Fig. 1. The difference between the two distributions in Fig. 3 is a result of the dynamics taking place when single atoms versus pairs of atoms are excited. Rydberg atoms expand from the excitation volume at the thermal velocity,  $\sim 8.9 \text{ cm s}^{-1}$  for Cs. Cs atom pairs expand at the vector sum of their thermal velocity, collisional recoil velocity and the velocity acquired from Coulomb repulsion after PFI. The molecular signal is much broader than the atomic signal, characteristic of the Coulomb repulsion between the ions created at close range,  $R \lesssim 10 \mu\text{m}$ , by PFI. Although the amplitude of the traces shown in Fig. 3 is similar, the count rates for the atomic signal are 3-4 orders of magnitude larger for identical excitation laser intensities.

The TOF distribution of a molecule will only be broadened by the thermal velocity and the velocity obtained from Coulomb repulsion because the collisional recoil velocity is zero. If the time between PFI and the average arrival time at the detector is not changed, the Coulomb repulsion between the atoms forming a molecule will remain constant as a function of  $\tau$  since the distribution of  $R$  remains constant. The TOF distribution under these conditions measures the distance between the excited atoms as a function of  $\tau$ . This description is valid as long as there is no observable wave-packet motion which would lead to an oscillating signal.

Pairs of atoms undergoing a collision have increasing internuclear separation,  $R$ , with increasing  $\tau$  so the Coulomb repulsion will decrease as  $\tau$  increases for fixed

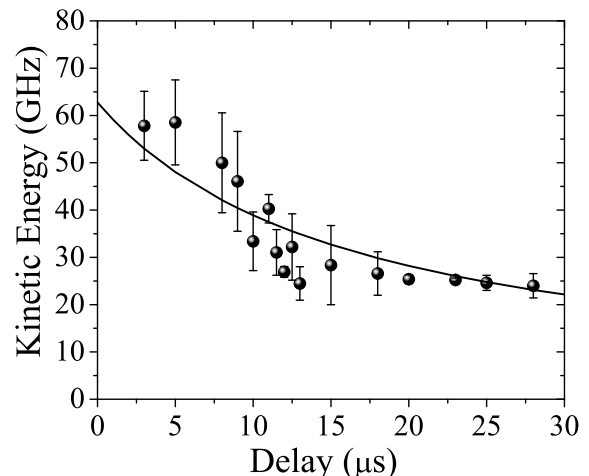


FIG. 4: This figure shows a plot of kinetic energy vs.  $\tau$  for a collision between two 89D atoms. The line is the energy expected for a pair of Cs atoms starting at  $R = 2.8 \mu\text{m}$  and moving uniformly apart at a velocity of  $17 \text{ cm s}^{-1}$  per atom for a time  $\tau$  before ionization as measured for this collision in [16].

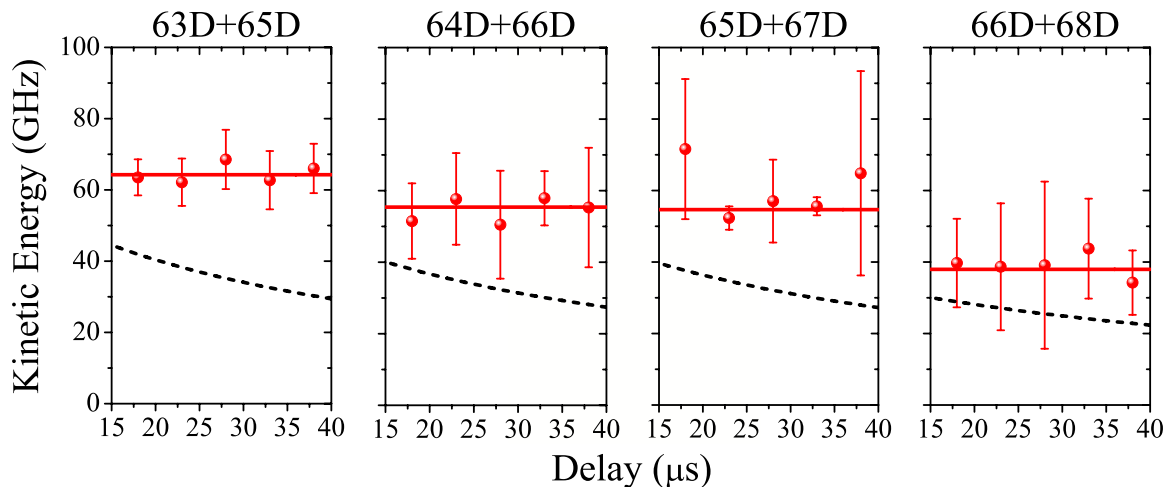


FIG. 5: Recoil kinetic energy vs. delay for  $63D + 65D$  with  $\epsilon = 224 \text{ mV cm}^{-1}$ ,  $64D + 66D$  with  $\epsilon = 205 \text{ mV cm}^{-1}$ ,  $65D + 67D$  with  $\epsilon = 190 \text{ mV cm}^{-1}$  and  $66D + 68D$  with  $\epsilon = 158 \text{ mV cm}^{-1}$ . Spheres denote the data taken for the molecular resonances and the dotted black line shows a calculation of the expected results of a binary collision with thermal velocity as described in the text.

TOF. An example of this behavior is shown in Fig. 4 for the collision between  $89D$  atoms studied in [16]. These dynamics will result in a Coulomb repulsion broadened TOF distribution at short  $\tau$  that becomes smaller as  $R$  increases due to the exit channel velocity of the fragments. Asymptotically,  $R \gtrsim 15 \mu\text{m}$ , when two atoms leaving a collision are ionized, the Coulomb repulsion is negligible and the velocity is determined by the exit channel velocity and sample temperature alone [16]. Collisions where the atoms are excited at long range and are allowed to evolve on attractive molecular potentials can also be studied in this way but this is a subject of future work.

To observe macrodimers, TOF distributions were acquired for  $\tau = 18 - 38 \mu\text{s}$ . Figure 5 shows the data for the 4 states used in the experiments. The times were chosen to be short enough to avoid decay of one of the molecular partners, but long enough to measure the dependence on  $\tau$  so that a collision could be distinguished from a macrodimer. The lifetime of a  $\sim 60D$  state including blackbody decay is  $\sim 100 \mu\text{s}$  [20, 21]. Qualitatively, the kinetic energy distribution is not changing with  $\tau$  indicating that the spectral feature that the laser is tuned to is a macrodimer.

A linear fit was applied to the data for each molecular pair shown in Fig. 5 to determine the minimum collision velocity that would give a similar TOF distribution. The velocity allowed by the experimental error in the measured distributions is  $0 \pm 1 \text{ cm s}^{-1}$  for  $63D + 65D$ ,  $-2.7 \pm 2.1 \text{ cm s}^{-1}$  for  $64D + 66D$ ,  $2.2 \pm 2.7 \text{ cm s}^{-1}$  for  $65D + 67D$  and  $3.4 \pm 4 \text{ cm s}^{-1}$  for  $66D + 68D$ . All errors quoted are standard deviations. The collision velocities are all zero within the resolution of our spectrometer,  $\sim 2.5 \text{ cm s}^{-1}$ , for all pairs [16, 18]. The noise in the mea-

surement increases with  $n$  because the molecular states are getting energetically closer to the nearest atomic line.

The data is also consistent with our calculations of the interatomic potential wells. Notice that the Coulomb repulsion decreases with increasing  $n$ . This is because the potential wells shift to larger  $R$  as  $n$  increases. The fact that the  $64D + 66D$  and  $65D + 67D$  macrodimers have approximately the same recoil kinetic energy is also predicted by our calculations. The  $R_e$  of the wells closest to the spectral lines studied at the  $\epsilon$  quoted in Fig. 5 for  $63D + 65D$ ,  $64D + 66D$ ,  $65D + 67D$ , and  $66D + 68D$  are approximately  $3.3 \mu\text{m}$ ,  $3.5 \mu\text{m}$ ,  $3.6 \mu\text{m}$  and  $3.9 \mu\text{m}$ , respectively. The  $R_e$  are a measure of the potential well shape. It should be pointed out, however, that most of the excitation probability is at large  $R$ . This is due to the Frank-Condon factors and the number of available pairs at particular  $R$  at our densities. These factors favor near dissociation states. The macrodimers spend most of their time at  $R = 4 - 9 \mu\text{m}$  at the outer turning points of the potential wells. We also note that there is not a simple  $n$  scaling law dependence to the well shape because this depends on  $\epsilon$  as well as  $n$ .

We compared the measured TOF distributions to simulations of the ion trajectories in our apparatus. Each simulation includes the spectrometer geometry,  $\epsilon$ , and the PFI pulse.  $R$  for each macrodimer was chosen uniformly from a range based on the calculated potential wells. Molecules or atoms were placed at random in the excitation volume according to the excitation laser intensity distribution. The simulated TOF distribution width was in good agreement with the molecular signal. The atomic measurement yields a  $\sim 50\%$  larger TOF distribution most likely due to the alignment of the dye laser focal spot to the MOT and the uncertainty in determin-

ing the laser spot size. The Coulomb repulsion for our range of  $\tau$  is at least 3 times larger than the thermal broadening so the spot size uncertainty does not prevent the measurement. The expected behavior shown in Fig. 4 as a solid line is also in good agreement with the data further verifying the accuracy of the simulations.

We compared the experimental data on the macrodimers to the expected behavior of an ultralow energy, 5.22 MHz, binary collision. The recoil velocity of the atom pair was taken to be equal to the thermal velocity of the cold gas and the initial  $R$  was set equal to that determined by the Coulomb repulsion measured in the experiment at the minimum  $\tau$ . The calculation is shown in Fig. 5 as a dotted line. The data from the experiment clearly indicates that the recoil velocity of the pair of atoms excited in the experiment is much less than the thermal velocity of the gas. Note that larger collision velocities cause the recoil kinetic energy from the Coulomb repulsion to decrease faster. This experimental result and the fact that our calculations predict bound states gives us confidence that we have observed bound macrodimers [16]. The measurement for 4 different states and the fact that the potential energy calculations predict potential wells that support bound states makes it highly unlikely that the laser, 1.5 MHz spectral bandwidth, could selectively excite pairs with relative velocities of  $< 3.4 \text{ m s}^{-1}$ .

## DISCUSSION

The potential wells probed in our experiment depend strongly on  $\epsilon$ . The resonances vanish at larger  $\epsilon$  because the potentials have become repulsive. At  $\epsilon = 0 \text{ mV cm}^{-1}$ , our calculations do not predict any of the prominent wells shown in Fig. 1 and the spectral features are not observed. In the cases explored in this paper, the molecular states are shifted as  $\epsilon$  is increased until they interact to form avoided crossings. As  $\epsilon$  is increased further, the states are shifted through each other so the bound states created by the avoided crossings are destroyed. The electric fields were chosen for our experiments so that the potential wells were broad and deep so that the molecules were most easily observed.

A closer look at the molecular signal in Fig. 3 indicates that there may be an alignment effect. The symmetric maxima about the peak center were observed for all the data. If there were no alignment effect, the TOF distribution would look flat topped with a smoothing from the thermal velocity [19]. We measured the TOF distribution for the molecular resonance with the dye laser polarization perpendicular to the TOF axis to explore this feature. We observed no difference in the width or shape of the distribution. We conclude that if alignment of the molecule is present, it is due to  $\epsilon$ . We currently have no way of verifying this conclusion without major

modifications to the apparatus. We plan to study this effect in the future.

To conclude, we have demonstrated the existence of bound molecular states of Cs Rydberg atom pairs by mapping the  $R$  distribution of the atoms using the Coulomb repulsion of the ions after PFI. Our experiments are in good agreement with Monte Carlo calculations using no adjustable parameters of the TOF distributions and calculations of the pair interactions of the Rydberg atoms. These macrodimers are stabilized by  $\epsilon$  and result from avoided crossings.  $\epsilon$  can be used to control the formation and characteristics of the molecules. Macrodimers like these will be observable in other species of cold Rydberg gases. With the higher densities that can be achieved in an optical dipole trap, imaging studies can be carried out to investigate the alignment effect noted here. Now that macrodimers have been observed, their production can be optimized and they can be trapped so these sensitive, novel states of matter can be used for new experiments.

## ACKNOWLEDGEMENTS

We acknowledge support from AFOSR (FA9550-05-0328) and ARO (W911NF-08-1-0257).

- 
- [1] Mourachko, I. et al. Many-body effects in a frozen Rydberg gas. *Phys. Rev. Lett.* **80**, 253 (1998).
  - [2] Anderson, W. R., Veale, J. R. & Gallagher, T. F. Resonant dipole-dipole energy transfer in a nearly frozen Rydberg gas. *Phys. Rev. Lett.* **80**, 249 (1998).
  - [3] Tong, D. et al. Local blockade of Rydberg excitations in an ultracold gas. *Phys. Rev. Lett.* **93**, 63001 (2004).
  - [4] Singer, K., Reetz-Lamour, M., Amthor, T., Marcassa, L. G. & Weidemüller, M. Suppression of excitation and spectral broadening induced by interactions in a cold gas of Rydberg atoms. *Phys. Rev. Lett.* **93**, 163001 (2004).
  - [5] Cubel Liebisch, T., Reinhard, A., Berman, P. R. & Raithel, G. Atom counting statistics in ensembles of interacting Rydberg atoms. *Phys. Rev. Lett.* **95**, 253002 (2005).
  - [6] Vogt, T. et al. Dipole blockade at Förster resonances in high resolution laser excitation of Rydberg states of Cesium atoms. *Phys. Rev. Lett.* **97**, 083003 (2006).
  - [7] Heidemann, R. et al. Evidence for coherent collective Rydberg excitation in the strong blockade regime. *Phys. Rev. Lett.* **99**, 163601 (2007).
  - [8] Jaksch, D. et al. Fast quantum gates for neutral atoms. *Phys. Rev. Lett.* **85**, 2208 (2000).
  - [9] Lukin, M. D. et al. Dipole blockade and quantum information processing in mesoscopic atomic ensembles. *Phys. Rev. Lett.* **87**, 37901 (2001).
  - [10] Brion, E., Molmer, K. & Saffman, M. Quantum computing with collective ensembles of multilevel systems. *Phys. Rev. Lett.* **99**, 260501 (2007).

- [11] Greene, C. H., Dickinson, A. S. & Sadeghpour, H. R. Creation of polar and nonpolar ultra-long-range Rydberg molecules. *Phys. Rev. Lett.* **85**, 2458 (2000).
- [12] Boisseau, C., Simbotin, I. & Cote, R. Macrodimers: ultralong range Rydberg molecules. *Phys. Rev. Lett.* **88**, 133004 (2002).
- [13] Schwettmann, A., Overstreet, K. R., Tallant, J. & Shaffer, J. P. Long range Cs Rydberg molecules. *J. Mod. Opt.* **54**, 2551 (2007).
- [14] Bendkowsky, V. et al. Observation of ultralong range Rydberg molecules. arXiv:0809.2961.
- [15] Farooqi, S. M. et al. Long-range molecular resonances in a cold Rydberg gas. *Phys. Rev. Lett.* **91**, 183002 (2003).
- [16] Overstreet, K. R., Schwettmann, A., Tallant, J. & Shaffer, J. P. Photoinitiated collisions between cold Cs Rydberg atoms. *Phys. Rev. A* **76**, 011403(R) (2007).
- [17] Schwettmann, A., Crawford, J., Overstreet, K. R. & Shaffer, J. P. Cold Cs Rydberg-gas interactions. *Phys. Rev. A* **74**, 020701(R) (2006).
- [18] Tallant, J., Overstreet, K. R., Schwettmann, A. & Shaffer, J. P. Sub-Doppler magneto-optical trap temperatures measured using Rydberg tagging. *Phys. Rev. A* **74**, 023410 (2006).
- [19] Mons, M. & Dimicoli, I. Angular correlation between photofragment velocity and angular momentum measured by resonance enhanced multiphoton ionization detection. *J. Chem. Phys.* **90**, 4037 (1989).
- [20] Farley, J. W. & Wing, W. H., Accurate calculation of dynamic Stark shifts and depopulation rates of Rydberg energy levels induced by blackbody radiation. Hydrogen, Helium, and Alkali-metal atoms. *Phys. Rev. A* **23**, 2397 (1981).
- [21] He, X., Li, B., Chen, A. & Zhang, C., Model-potential calculation of lifetimes of Rydberg states of Alkali atoms. *J. Phys. B* **23**, 661 (1990).